



THE UNIVERSITY *of* EDINBURGH

## Edinburgh Research Explorer

### Inertia-gravity-wave radiation by a sheared vortex

**Citation for published version:**

Olafsdottir, EI, Olde Daalhuis, AB & Vanneste, J 2008, 'Inertia-gravity-wave radiation by a sheared vortex', *Journal of Fluid Mechanics*, vol. 596, no. n/a, pp. 169-189. <https://doi.org/10.1017/S0022112007009408>

**Digital Object Identifier (DOI):**

[10.1017/S0022112007009408](https://doi.org/10.1017/S0022112007009408)

**Link:**

[Link to publication record in Edinburgh Research Explorer](#)

**Document Version:**

Publisher's PDF, also known as Version of record

**Published In:**

Journal of Fluid Mechanics

**General rights**

Copyright for the publications made accessible via the Edinburgh Research Explorer is retained by the author(s) and / or other copyright owners and it is a condition of accessing these publications that users recognise and abide by the legal requirements associated with these rights.

**Take down policy**

The University of Edinburgh has made every reasonable effort to ensure that Edinburgh Research Explorer content complies with UK legislation. If you believe that the public display of this file breaches copyright please contact [openaccess@ed.ac.uk](mailto:openaccess@ed.ac.uk) providing details, and we will remove access to the work immediately and investigate your claim.



# Inertia–gravity-wave radiation by a sheared vortex

E. I. ÓLAFSDÓTTIR, A. B. OLDE DAALHUIS  
AND J. VANNESTE

School of Mathematics and Maxwell Institute for Mathematical Sciences, University of Edinburgh,  
Edinburgh EH9 3JZ, UK

(Received 4 June 2007 and in revised form 27 September 2007)

We consider the linear evolution of a localized vortex with Gaussian potential vorticity that is superposed on a horizontal Couette flow in a rapidly rotating strongly stratified fluid. The Rossby number, defined as the ratio of the shear of the Couette flow to the Coriolis frequency, is assumed small. Our focus is on the inertia–gravity waves that are generated spontaneously during the evolution of the vortex. These are exponentially small in the Rossby number and hence are neglected in balanced models such as the quasi-geostrophic model and its higher-order generalizations. We develop an exponential-asymptotic approach, based on an expansion in sheared modes, to give an analytic description of the three-dimensional structure of the inertia–gravity waves emitted by the vortex. This provides an explicit example of the spontaneous radiation of inertia–gravity waves by localized balanced motion in the small-Rossby-number regime.

The inertia–gravity waves are emitted as a burst of four wavepackets propagating downstream of the vortex. The approach employed reduces the computation of inertia–gravity-wave fields to a single quadrature, carried out numerically, for each spatial location and each time. This makes it possible to unambiguously define an initial state that is entirely free of inertia–gravity waves, and circumvents the difficulties generally associated with the separation between balanced motion and inertia–gravity waves.

---

## 1. Introduction

The fast rotation and strong stratification of the atmosphere and oceans lead to a time-scale separation between the slow advective motion termed balanced motion on the one hand, and the fast inertia–gravity waves (IGWs) on the other hand. Because of this time-scale separation, the interactions between the two types of motion are weak, and to a first approximation at least, the balanced motion evolves independently from the IGWs. This feature, now well supported by a number of theoretical studies (e.g. Babin, Mahalov & Nicolaenko 2000; Majda & Embid 1998; Reznik, Zeitlin & Ben Jelloul 2001), is a first key to the usefulness of balanced models, which filter out IGWs; a second is the observation that, largely because of the low-frequency nature of the large-scale forcing, the IGW activity is weak in many parts of the atmosphere and oceans (ignoring tidal motion). That is not to say, however, that IGWs can be neglected in all circumstances: they are crucial, for instance, to the middle-atmospheric circulation and to oceanic mixing. As a result, there is a strong interest in identifying and studying the mechanisms of IGW generation (e.g. Fritts & Alexander 2003).

The so-called spontaneous generation is one such mechanism which has attracted a great deal of attention in recent years. This describes the way in which the natural evolution of a balanced flow leads to the emission of IGWs. It should be contrasted with the generation of IGWs caused by the adjustment of a flow that is initially unbalanced (e.g. Reznik *et al.* 2001, and references therein). Spontaneous generation is now well understood in the small-Froude-number regime, where it is caused by Lighthill-like radiation of IGWs with asymptotically large spatial scales and, hence, frequencies that match those of the balanced motion (e.g. Ford, McIntyre & Norton 2000; Plougonven & Zeitlin 2002). Less well understood is the arguably more relevant small-Rossby-number regime, where there is a frequency gap between IGWs of all scales and balanced motion. On the basis of simple mechanistic models, governed by ordinary differential equations (ODEs; Lorenz & Krishnamurthy 1987; Warn 1997; Vanneste 2004, 2008), it has been argued that the IGW generation in this regime is exponentially weak in the Rossby number. This leads to a number of subtle issues (such as the unambiguous separation between balanced motion and IGWs) which, although largely resolved for ODE models, remain challenging for the partial differential equations governing realistic geophysical flows. Even the direct numerical simulation of IGW generation in idealized flows at small Rossby number has proved highly delicate, and it is only in the last few years that reliable results, in particular on the IGWs emitted in baroclinic life cycles, have been obtained (e.g. O'Sullivan & Dunkerton 1995; Zhang 2004; Plougonven & Snyder 2005, 2007; Viúdez & Dritschel 2006; Viúdez 2006). These results are still partial, however, and do not answer such fundamental questions as the Rossby-number dependence of the IGW amplitudes.

Therefore, there is a need for analytic treatments which give a precise description of IGW generation in simple model flows. Such a treatment was provided by Vanneste & Yavneh (2004) and Ólafsdóttir, Olde Daalhuis & Vanneste (2005) who use exponential-asymptotic techniques to estimate the amplitude of the IGW oscillations that appear in the evolution of a Couette flow perturbed by sheared modes, that is, plane waves with time-dependent wavenumber in the cross-stream direction. In this paper, we make use of their results to compute the IGWs generated in a more realistic flow. Specifically, we study the IGWs that are radiated when a three-dimensional vortex is sheared by a Couette flow. This is a significant step toward the application of exponential asymptotics to realistic flows, particularly because the vortex and hence the region of wave generation are localized in space. This is in contrast with the sheared modes of Vanneste & Yavneh (2004) which have infinite energy. The process that we examine may also be argued to occur in the atmosphere and oceans, where vortices and large-scale shear are commonplace.

Our analysis takes as its starting point the equations of motion for a rotating stratified fluid under the Boussinesq and hydrostatic approximations. We consider the linear evolution of a vortex with Gaussian potential vorticity placed in a uniform horizontal shear flow. The ratio of the shear amplitude to the Coriolis frequency defines a Rossby number  $\varepsilon$  which is assumed to be small. In terms of potential vorticity, the evolution is trivial: the ellipsoidal surfaces of constant potential vorticity are deformed advectively, with their semi-axes slowly expanding and contracting whilst tilting in the horizontal plane. In the quasi-geostrophic approximation, and indeed in any balanced approximation, all the dynamical fields are slaved to the potential vorticity and hence undergo an analogous slow evolution. In the full Boussinesq model, however, exponentially small IGWs are emitted by the vortex and radiate

away rapidly. We use an exponential-asymptotic approach to provide a largely analytic description of these waves.

Our approach relies on the fact that, at a linear level, a localized disturbance in a Couette flow can be described as a superposition of independently evolving sheared modes. As mentioned above, the generation of IGW-like oscillations by a single sheared mode has been studied by Vanneste & Yavneh (2004) and Ólafsdóttir *et al.* (2005). They show how fast IGW oscillations are switched on through a Stokes phenomenon, which occurs precisely when the phase lines of the sheared mode are perpendicular to the Couette flow, and they derive an analytic expression for the amplitude of the IGW oscillations. Superposing the IGW contributions of a continuum of sheared modes, we obtain an approximation for the IGW field generated by a vortex as a triple integral. Approximating this by a combination of asymptotic and numerical means provides a detailed description of the structure of the IGWs emitted. This takes the form of four wavepackets which are generated when the horizontal semi-axes of the ellipsoid are approximately aligned with the streamwise and cross-stream directions. Subsequently these wavepackets propagate horizontally and vertically in the background shear.

It is worth emphasizing that our analytic approach eliminates most of the conceptual difficulties encountered when attempting to demonstrate spontaneous IGW generation. In particular, the asymptotic treatment makes it possible to define an initial state of the vortex that is completely balanced. More precisely, the imbalance at the initial time is negligible compared to the smallest terms captured by our asymptotic approach, namely the exponentially small IGWs that appear afterwards. These IGWs can then be unambiguously identified as resulting from spontaneous generation. The IGWs are also completely disentangled from the balanced motion, which we do not describe in detail. This state of affairs contrasts sharply with more numerical treatments of the problem of IGW generation, where sophisticated methods are required both for the initialization of the balanced state and for the diagnosis of the IGWs generated (cf. Viúdez & Dritschel 2004). Of course, a limitation of our treatment is that, so far, it applies to very specific flows and under the severe restriction of linearization.

This paper is organized as follows. The equations of motion and the special solution under study are introduced in §2. The expansion of this solution in terms of sheared modes and the choice of potential-vorticity distribution are discussed in §3. The asymptotic analysis leading to the explicit description of the IGWs is described in §4. There we review the relevant exponential-asymptotic results for sheared modes, exploit them to express the vertical vorticity associated with IGWs as a triple integral, and sketch the method used to estimate this integral. Some results, illustrating the spontaneous generation of IGWs in an anticyclonic flow, are presented in §5. The paper concludes with a discussion in §6. A large part of the work reported in this paper is rather technical. Therefore §§3–4 only summarize the method employed, and we refer the reader to the two appendices for a more detailed analysis.

## 2. Model

We study the spontaneous generation of inertia–gravity waves by a slow balanced motion in a rotating stratified fluid. The fluid domain is assumed to be unbounded in the three spatial dimensions. We model the fluid using the Boussinesq and hydrostatic

approximations and write the equations of motion as

$$D_t U - fV = -\Phi_x, \quad (2.1)$$

$$D_t V + fU = -\Phi_y, \quad (2.2)$$

$$B = \Phi_z, \quad (2.3)$$

$$D_t B + N^2 W = 0, \quad (2.4)$$

$$U_x + V_y + W_z = 0. \quad (2.5)$$

Here  $\mathbf{U} = (U, V, W)$  are the usual Cartesian components of the velocity,  $D_t = \partial_t + \mathbf{U} \cdot \nabla$  is the material derivative,  $f$  is the Coriolis parameter,  $\Phi$  is the geopotential, related to the pressure  $P$  and constant mean density  $\bar{\rho}$  by  $P = \Phi/\bar{\rho}$ ,  $B = -g\rho/\bar{\rho}$  is the buoyancy (with  $\rho$  the density perturbation), and  $N$  is the constant Brunt–Väisälä frequency. Note that the hydrostatic approximation is made for convenience only; no conceptual difficulties would arise if it were relaxed, although the computations would be considerably more involved.

We consider solutions of (2.1)–(2.5) which consist of two parts: a horizontal Couette flow, with constant vorticity  $-\Sigma$ , and a small-amplitude perturbation. We therefore write the dynamical fields as

$$(U, V, W, \Phi, B) = \left( \Sigma y, 0, 0, -\frac{f\Sigma y^2}{2}, 0 \right) + (u(x, y, z, t), v(x, y, z, t), w(x, y, z, t), \varphi(x, y, z, t), b(x, y, z, t)), \quad (2.6)$$

and derive linearized equations of motion for the perturbation fields  $(u, v, w, \phi, b)$ . These equations are identical to (2.1)–(2.5), with upper-case variables replaced by their lower-case counterparts, and  $D_t = \partial_t + \Sigma y \partial_x$ . They imply that the potential-vorticity perturbation

$$q = N^2 \zeta + (f - \Sigma)b_z,$$

is conserved:

$$D_t q = (\partial_t + \Sigma y \partial_x)q = 0, \quad \text{hence} \quad q(x, y, z, t) = q_0(x - \Sigma y t, y, z), \quad (2.7)$$

where  $q_0$  is the initial distribution of  $q$ . Note that the linearization of (2.1)–(2.5) is justified if the vertical vorticity associated with  $q_0$  is negligible compared to the background vorticity  $\Sigma$ , that is, if  $q_0/N^2 \ll \Sigma$ . We assume that this condition holds.

Although the approach of this paper applies to arbitrary localized distributions of potential vorticity, we concentrate in what follows on a particularly simple situation where  $q_0$  is given by

$$q_0(x, y, z) = \frac{\pi^{3/2} N f}{2^3 \alpha_1 \alpha_2 \alpha_3} \exp \left\{ - \left[ \frac{(x + \Sigma T y)^2}{4\alpha_1^2} + \frac{y^2}{4\alpha_2^2} + \frac{z^2}{4\alpha_3^2} \right] \right\}, \quad (2.8)$$

where  $\alpha_i$ ,  $i = 1, 2, 3$  and  $T$  are constants, and the factor  $\pi^{3/2} N f / (2^3 \alpha_1 \alpha_2 \alpha_3)$  is introduced for later convenience. To write  $q_0$  in this form, we have taken advantage of the linearity of the problem: the right-hand side of (2.8) should be multiplied by a constant, with dimension of  $(\text{length})^3 \times (\text{time})^{-1}$ , to obtain a dimensionally consistent potential vorticity of any desired amplitude.

According to (2.7), the potential vorticity at later time is given by

$$q(x, y, z, t) = \frac{\pi^{3/2} N f}{2^3 \alpha_1 \alpha_2 \alpha_3} \exp \left\{ - \left[ \frac{(x - \Sigma(t - T)y)^2}{4\alpha_1^2} + \frac{y^2}{4\alpha_2^2} + \frac{z^2}{4\alpha_3^2} \right] \right\}. \quad (2.9)$$

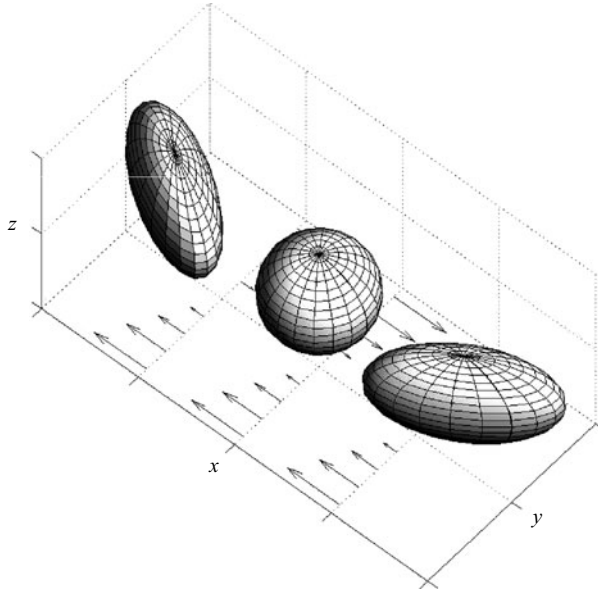


FIGURE 1. Schematic of the evolution of the perturbation potential vorticity  $q$  in the Couette flow for  $\Sigma > 0$  and  $T > 0$ . The leftmost surface represents a particular level surface of  $q$  at  $t = 0$  when level surfaces are ellipsoids tilted against the shear; the central sphere represents the same level surface at  $t = T$  when level surfaces are ellipsoids with axes aligned with the coordinate axes; the rightmost surface represents the level surface at  $t > T$  when level surfaces are ellipsoids tilted with the shear. The centres of the ellipsoids, which are fixed in time, have been offset in the  $x$ -direction for clarity.

This describes a three-dimensional Gaussian vortex which becomes deformed and tilted in the horizontal under the action of the Couette flow, see figure 1. The parameter  $T$  controls the initial tilt against the shear and is such that the three axes of the ellipsoidal level surfaces of  $q$  are aligned with the  $(x, y, z)$ -axes at  $t = T$ . If  $\alpha_1 = \alpha_2 = \alpha_3$ , in particular,  $q$  is spherically symmetric at  $t = T$ . The parameter  $T$  is introduced so that we can vary the shape of the ellipsoid at the time, taken to be  $t = 0$ , when the solution will be assumed to be perfectly balanced.

Our interest is in the behaviour of dynamical fields which, unlike  $q$ , can display IGW activity. We focus on the rotation-dominated regime where the Rossby number, naturally defined as

$$\varepsilon = \frac{|\Sigma|}{f},$$

is small. In this regime, suitably initialized flows are described well by balanced models (quasi-geostrophic and higher order) which filter out IGWs completely (e.g. Warn *et al.* 1995). In these models all the dynamical fields can be deduced from  $q$  and so, apart from fine details depending on each specific balanced model, their evolution is completely understood from (2.9). In the rest of the paper we demonstrate how IGWs, not captured by balanced models, are emitted spontaneously in the course of this evolution. We describe these IGWs using an asymptotic method and show that they are exponentially small in  $\varepsilon$ .

### 3. Sheared modes

Small-amplitude perturbations to a Couette flow which are localized in space can be conveniently represented as superpositions of sheared modes; specifically, the perturbation fields can be written as

$$u(x, y, z, t) = \int_{\mathbb{R}^3} \hat{u}(k, l, m, t) \exp[i(kx + (l - k\Sigma t)y + mz)] dk dl dm, \quad (3.1)$$

with similar expressions for  $v$ ,  $w$ ,  $\phi$  and  $b$ . Note that this representation differs from the usual Fourier transform in that the wavevector associated with each mode and given by  $(k, l - k\Sigma t, m)$  depends on time.

Introducing the expansion (3.1) into the linearized perturbation equations leads to a system of ODEs in time for the amplitudes  $(\hat{u}, \hat{v}, \hat{w}, \hat{\phi}, \hat{b})$ , with  $(k, l, m)$  appearing as parameters. This system of ODEs is derived in McWilliams & Yavneh (1998), Vanneste & Yavneh (2004) (for non-hydrostatic flows), and Ólafsdóttir *et al.* (2005). It reduces to a single second-order equation for the amplitude

$$\hat{\zeta} = ik\hat{v} - i(l - \Sigma kt)\hat{u}$$

of the vertical component of the perturbation vorticity. This reduction relies on the conservation (2.7) of the potential vorticity. In terms of the amplitude  $\hat{q}$  of  $q$  in the sheared-mode expansion, this conservation becomes

$$\hat{q}_t = 0, \quad \text{hence} \quad \hat{q}(k, l, m, t) = \hat{q}_0(k, l, m), \quad (3.2)$$

where  $\hat{q}_0$  is the Fourier transform of  $q_0$ . From (2.8), we find  $\hat{q}_0$  to be given by

$$\hat{q}_0(k, l, m) = Nf \exp \left\{ -[\alpha_1^2 k^2 + \alpha_2^2 (l - k\Sigma T)^2 + \alpha_3^2 m^2] \right\}. \quad (3.3)$$

Taking (3.2) into account, and non-dimensionalizing time by the inverse shear  $|\Sigma|$  leads to the following ODE for  $\hat{\zeta}$  (see e.g. Vanneste & Yavneh (2004) or Ólafsdóttir *et al.* (2005) for a derivation):

$$\varepsilon^2 [\hat{\zeta}_{tt} + b(t - \sigma l/k) \hat{\zeta}_t] + c(t - \sigma l/k) \hat{\zeta} = \frac{1 + (t - \sigma l/k)^2}{N^2 \beta^2} \hat{q}_0, \quad (3.4)$$

where

$$b(t) = -\frac{2t}{1 + t^2}, \quad (3.5)$$

$$c(t) = (1 - \sigma\varepsilon) \left( 1 - \frac{2\sigma\varepsilon}{1 + t^2} \right) + \frac{1 + t^2}{\beta^2}, \quad (3.6)$$

and  $\sigma = \text{sign } \Sigma$  indicates whether the shear is anticyclonic ( $\sigma = 1$ ) or cyclonic ( $\sigma = -1$ ). A second non-dimensional number appears in (3.4) in addition to  $\varepsilon$ , namely

$$\beta = \frac{fm}{Nk},$$

which can be interpreted as the inverse square-root of a Burger number and will be treated as  $O(1)$ .

Now, the explicit dependence of (3.4) on  $\sigma l/k$ ,  $\hat{q}_0$  and  $N^2$  is readily eliminated by introducing the new dependent variable  $\tilde{\zeta}(k, l, m, t)$  defined by

$$\begin{aligned} \hat{\zeta}(k, l, m, t) &= \frac{\hat{q}_0}{N^2} \tilde{\zeta}(k, l, m, t - \sigma l/k) \\ &= \frac{f}{N} \exp \left\{ -[\alpha_1^2 k^2 + \alpha_2^2 (l - k\sigma T)^2 + \alpha_3^2 m^2] \right\} \tilde{\zeta}(k, l, m, t - \sigma l/k), \end{aligned} \quad (3.7)$$

where  $T$  has also been non-dimensionalized by  $|\Sigma|$ . Using (3.2), this transformation reduces (3.4) to

$$\varepsilon^2 \left( \frac{d^2 \tilde{\zeta}}{dt^2} + b(t) \frac{d\tilde{\zeta}}{dt} \right) + c(t) \tilde{\zeta} = \frac{1+t^2}{\beta^2}, \quad (3.8)$$

with  $b(t)$  and  $c(t)$  still given by (3.5)–(3.6). This equation is the hydrostatic limit of that derived by McWilliams & Yavneh (1998) and Vanneste & Yavneh (2004). It is identical to that derived by Ólafsdóttir *et al.* (2005). These three papers focused on a single sheared mode, that is, on a single wavevector  $(k, l, m)$ . Here we exploit the asymptotic results of the latter two papers to compute the vertical component of the vorticity  $\zeta(x, y, z, t)$  associated with a localized potential vorticity perturbation. According to (3.7), it is related to the solutions of (3.8) obtained for different values of  $(k, l, m)$  by

$$\begin{aligned} \zeta(x, y, z, t) = & \frac{1}{N^2} \int_{\mathbb{R}^3} \hat{q}_0(k, l, m) \tilde{\zeta}(k, l, m, t - \sigma l/k) \\ & \times \exp[i(kx + (l - k\Sigma t)y + mz)] dk dl dm. \end{aligned} \quad (3.9)$$

We now use an explicit asymptotic form for  $\tilde{\zeta}$  to derive an approximation to the IGW component of  $\zeta(x, y, z, t)$ .

#### 4. Asymptotic analysis

In Ólafsdóttir *et al.* (2005), it is shown that solutions of (3.8) which are well balanced for  $t < 0$  develop fast IGW oscillations for  $t > 0$ . This generation of oscillations can be identified as a Stokes phenomenon: a well-balanced, oscillation-free dominant solution of (3.8) switches on a subdominant homogeneous solution as the Stokes line  $\text{Re } t = 0$  is crossed. The switching on is continuous (Berry 1989), but takes place over a short time, of  $O(\varepsilon^{1/2})$ , so we can write the solution as

$$\tilde{\zeta}(k, l, m, t) = \tilde{\zeta}_{\text{bal}}(\beta, t) + \tilde{\zeta}_{\text{igw}}(\beta, t)H(t), \quad (4.1)$$

where  $H(t)$  denotes the Heaviside function and the notation emphasizes that  $\tilde{\zeta}_{\text{bal}}$  and  $\tilde{\zeta}_{\text{igw}}$  depend on  $(k, l, m)$  through  $\beta$  only. The balanced part  $\tilde{\zeta}_{\text{bal}}$  of the solution is given by an asymptotic series whose details are unimportant for our purpose. The IGW part, which is a homogeneous solution of (3.8), is given to leading order in  $\varepsilon$  by

$$\begin{aligned} \tilde{\zeta}_{\text{igw}}(\beta, t) \sim & -\sqrt{\frac{2|\beta|\pi}{\varepsilon}} \exp[-\pi(1 + \beta^2 - \sigma\beta^2\varepsilon)/(4|\beta|\varepsilon)] \\ & \times \frac{\sqrt{1 + \beta^2 + t^2} \sin R(t, \varepsilon) - \sigma|\beta|t \cos R(t, \varepsilon)}{(1 + \beta^2 + t^2)^{1/4}(1 + \beta^2)^{3/4}}, \end{aligned} \quad (4.2)$$

where

$$\begin{aligned} R(t, \varepsilon) = & \frac{1}{2|\beta|\varepsilon} \left( t\sqrt{1 + \beta^2 + t^2} + (1 + \beta^2) \ln \left( \frac{t + \sqrt{1 + \beta^2 + t^2}}{\sqrt{1 + \beta^2}} \right) \right) \\ & - \frac{\sigma|\beta|}{2} \ln \left( \frac{t + \sqrt{1 + \beta^2 + t^2}}{\sqrt{1 + \beta^2}} \right). \end{aligned}$$

Note that Ólafsdóttir *et al.* (2005, equations (4.7) and (4.8)) give this result for  $\sigma = -1$  only (with a typo in the argument of the exponential independent of  $\varepsilon$ ); the derivation



is however readily extended to the case  $\sigma = 1$ . Note also that

$$\frac{dR}{dt}(t, \varepsilon) = \frac{\sqrt{1 + \beta^2 + t^2}}{|\beta|\varepsilon} + O(1)$$

can be recognized as the non-dimensional frequency of hydrostatic IGWs with wavevector  $(k, -\sigma kt, m)$ .

Together with (3.9), (4.2) provides an explicit expression for the IGW part of  $\zeta(x, y, z, t)$ . Some care is needed, however, to ensure that meaningful initial conditions are satisfied at  $t = 0$ . Equations (4.1)–(4.2) are obtained assuming that there are no IGW oscillations for  $t < 0$ , at least to the level of accuracy of the asymptotic approximation (4.2). They then describe the spontaneous generation of oscillations that are present for  $t > 0$ . The shift of  $t$  by  $\sigma l/k$  involved in (3.9) means that different sheared modes, with different  $l/k$ , generate oscillations at different times. In particular, modes with  $\sigma l/k < 0$  generate oscillations for  $t < 0$ . This is problematic since it implies that IGWs are present at all times, when a natural initial condition is that the flow is completely balanced, that is, completely free of IGWs, at  $t = 0$ . Indeed, we want to ensure that the IGW activity vanishes in the limit  $t \rightarrow 0$ , so that the subsequent IGW generation is genuinely spontaneous. This condition can be imposed without difficulty by recognizing that one can add to (4.1) arbitrary combinations of the homogeneous solutions of (3.8), hence, in particular, an arbitrary multiple of  $\tilde{\zeta}_{\text{igw}}$ . Thus, we replace (4.1) by

$$\tilde{\zeta}(k, l, m, t) = \tilde{\zeta}_{\text{bal}}(\beta, t) + \tilde{\zeta}_{\text{igw}}(\beta, t)[H(t) + C(k, l, m)], \quad (4.3)$$

and choose  $C(k, l, m)$  to eliminate the IGW component of  $\zeta(x, y, z, t)$  for  $t = 0$ . It is clear from (3.9) that this is achieved by taking

$$C(k, l, m) = -1 \quad \text{for } \sigma l/k < 0 \quad \text{and} \quad C(k, l, m) = 0 \quad \text{for } \sigma l/k > 0. \quad (4.4)$$

For  $t \geq 0$ , this ensures that the sheared modes with  $\sigma l/k < 0$ , for which IGW oscillations appear for some  $t < 0$ , do not contribute to (3.9), while the modes with  $\sigma l/k > 0$  contribute for  $t > \sigma l/k$ . It may be helpful to think of (4.4) as imposing a certain amount of IGW activity as  $t \rightarrow -\infty$ ; this is chosen to precisely cancel the activity generated spontaneously for  $-\infty < t < 0$  and hence to lead to a completely balanced state at  $t = 0$ .

With the choice (4.3)–(4.4) and for  $t \geq 0$ , (3.9) becomes

$$\begin{aligned} \zeta(x, y, z, t) &= \frac{1}{N^2} \int_{\mathbb{R}^3} \hat{q}_0(k, l, m) \tilde{\zeta}_{\text{bal}}(\beta, t - \sigma l/k) \exp[i(kx + (l - \sigma kt)y + mz)] dk dl dm \\ &\quad + \frac{\sigma}{N^2} \int_{-\infty}^{\infty} \left( \int_{-\infty}^0 \int_{\sigma kt}^0 + \int_0^{\infty} \int_0^{\sigma kt} \right) \hat{q}_0(k, l, m) \\ &\quad \times \tilde{\zeta}_{\text{igw}}(\beta, t - \sigma l/k) \exp[i(kx + (l - \sigma kt)y + mz)] dl dk dm \end{aligned} \quad (4.5)$$

$$= \zeta_{\text{bal}}(x, y, z, t) + \zeta_{\text{igw}}(x, y, z, t). \quad (4.6)$$

We focus on the IGW component which, taking (3.3) into account, takes the more explicit form

$$\begin{aligned} \zeta_{\text{igw}}(x, y, z, t) &= \frac{\sigma f}{N} \int_{-\infty}^{\infty} \left( \int_{-\infty}^0 \int_{\sigma kt}^0 + \int_0^{\infty} \int_0^{\sigma kt} \right) \tilde{\zeta}_{\text{igw}}(\beta, t - \sigma l/k) \\ &\quad \times \exp \left\{ -[\alpha_1^2 k^2 + \alpha_2^2 (l - k\sigma T)^2 + \alpha_3^2 m^2] \right. \\ &\quad \left. + i(kx + (l - \sigma kt)y + mz) \right\} dl dk dm, \end{aligned} \quad (4.7)$$

with  $\tilde{\zeta}_{\text{igw}}$  given in (4.2). This is a closed-form expression for the IGWs radiated spontaneously by the sheared vortex in the limit  $\varepsilon \ll 1$ . Four observations can be made about this expression. First, it is clear that  $\lim_{t \rightarrow 0} \zeta_{\text{igw}} = 0$ : as expected, the vortex is well balanced at  $t=0$ , and the IGWs appear smoothly for  $t > 0$ . Second, it is obvious from (4.2) that  $\zeta_{\text{igw}}$  is exponentially small in  $\varepsilon$ . A crude estimate for its magnitude, based on the maximum amplitude of  $\tilde{\zeta}_{\text{igw}}$  (attained for  $|\beta|=1$ ), is  $\exp[-\pi/(2\varepsilon)]$ . This gives a rough idea of the importance of the IGWs radiated, even though the exponential dependence of  $\zeta_{\text{igw}}$  on  $\varepsilon$  depends of course on  $(x, y, z, t)$ . A third observation is that, because of the  $O(1)$  prefactor in (4.2), the IGW amplitude is larger for an anticyclonic shear ( $\sigma = 1$ ) than for a cyclonic shear ( $\sigma = -1$ ). A fourth observation relates to the role of the parameter  $T$  controlling the initial tilt of the potential-vorticity distribution against the shear. Consider the case where  $T > 0$ , so that the ellipsoidal vortex is initially tilted against the shear. It can be seen from (4.7) that the dominant contribution to  $\zeta_{\text{igw}}$  comes from wavenumbers satisfying  $l \approx \sigma k T$ . Since phase cancellations are minimized in the integral for  $l = \sigma k t$ , we can expect the maximum of IGW generation for  $t \approx T$ , that is, around the time when the axes of the constant-potential-vorticity ellipsoids are parallel to the coordinate axes. This can also be explained as follows. Each sheared mode leads to the generation of IGW oscillations at the ‘Stokes’ time  $\sigma l/k$ . The time of maximum IGW generation can be expected to coincide with the ‘Stokes’ time of the modes with the largest amplitudes, namely the modes with  $l = k\sigma T$  (cf. (3.3)), leading to  $t \approx T$  for the maximum generation. A reason for introducing the parameter  $T$  is that by taking  $T$  large enough, we can ensure a good separation between the initial time, when we impose the absence of any IGWs, and the time at which significant wave generation occurs. The picture of the IGW generation that is obtained in this case is then approximately independent of the specific choice of  $T$ , or in other words, of the specific shape of the potential-vorticity ellipsoid at the time  $t=0$  when we choose to impose that IGWs are absent. Physically, this is related to the fact that a large  $T$  corresponds at  $t=0$  to highly elongated ellipsoids which have little dynamical activity (since the associated velocity field is weak) and hence are well balanced.

To evaluate (4.9) in practice, it is necessary to make further analytical progress in order to limit the amount of computation required. We proceed in four steps: (i) the integration variables in (4.9) are changed from  $(k, l, m)$  to  $(k, \beta, \tau)$ , with  $\tau = t - \sigma l/k$ ; (ii) the integration with respect to  $k$  is carried out explicitly; (iii) an asymptotic method is used to approximate the integral with respect to  $\tau$ ; and (iv) the final integration with respect to  $\beta$  is computed numerically. Details of the necessary calculations are given in Appendix A.

The most delicate point in these calculations arises in step (iii) where the integral in  $\tau$  is found to be dominated either by a saddle point or by one of the two endpoints  $\tau = 0$  and  $\tau = t$ , depending on  $(x, y, z, t)$ . To deal with this, we have implemented a version of Bleistein’s (1966) method which gives a uniform approximation to this type of integral and is discussed in Appendix B. Note that the saddle point needs to be determined numerically for each value of  $(x, y, z, t)$  and  $\beta$ .

An important outcome of the asymptotic treatment in (iii) is that for  $t = O(1)$   $\zeta_{\text{igw}}$  varies over spatial scales of the order of  $\varepsilon^{-1/2}$ , much larger than the vortex scale. An identical scaling has been found in Vanneste (2006) in a much simpler model of IGW radiation. The IGW-like waves considered in that paper are one-dimensional, with dispersion relation  $\omega = \pm (1 + k^2)^{1/2}/\varepsilon$ , and their amplitude is proportional to  $\exp(-\alpha\omega)$  for some wavenumber-independent constant  $\alpha > 0$ . In this case, it is straightforward to see that the wave-radiation process is dominated by waves with

small  $k$  corresponding to the minimum of  $\omega$ . More precisely, since  $\omega(k) \approx (1 + k^2/2)/\varepsilon$  for  $k \approx 0$ , an  $O(\varepsilon^{1/2})$  neighbourhood of  $k=0$  dominates, leading to the  $\varepsilon^{-1/2}$  scaling for the spatial dependence of the waves. The present situation is more complex, with sheared modes that have time-dependent frequencies, and amplitudes that cannot be related so simply to frequencies. However, it is similarly a small  $O(\varepsilon^{1/2})$  neighbourhood of the wavenumbers  $k=m=0$  (with  $\beta \approx 1$ ) which is found to dominate the IGW generation process.

In the next section, we present some illustrative results of our approach and describe the structure of the IGWs generated by a vortex.

## 5. Results

We report results obtained for  $T=3$  in the case  $\sigma=1$ , that is for an anticyclonic flow. Our choice of the ellipsoidal potential vorticity (2.9) takes the semi-axes to be  $\alpha_1=\alpha_2=1$  and  $\alpha_3=f/N$ . This implies that at the time  $t=T=3$ , when maximum wave generation can be expected, the potential-vorticity distribution is spherically symmetric in coordinates stretched by the Prandtl ratio  $N/f$  in the vertical.

We have chosen to present results for the Rossby number  $\varepsilon=0.25$ . This is a moderately small value, giving significant amplitudes for the IGW generated, but also a value for which our asymptotic approximations have a reasonably good accuracy. Qualitatively, the results for other values of  $\varepsilon$  are similar, except that the amplitude of the IGWs radiated increases rapidly with  $\varepsilon$  as expected from the order of magnitude  $\exp[-\pi/(2\varepsilon)]$ .

As mentioned above and discussed in more detail in Appendix A, the spatial scale of the IGWs radiated by the vortex is  $\varepsilon^{-1/2}$ . Furthermore, the vertical dependence is through  $Nz/f$  (see (A 1)–(A 2)). It is then natural to regard the spatial structure of the IGWs as depending of the scaled coordinates  $(X, Y, Z) = \varepsilon^{1/2}(x, y, Nz/f)$ . With the choice  $\alpha_3 = N/f$ , the vertical vorticity  $\zeta_{\text{igw}}(X, Y, Z, t)$  becomes independent of  $f$  and  $N$ .

For both the computation and the presentation of the results, we can take advantage of symmetries of the problem:  $\zeta_{\text{igw}}$  is left invariant by the reflection about the plane  $z=0$  and by the rotation by  $\pi$  around the  $z$ -axis. Because the IGWs are also very weak upstream of the vortex, we can restrict our attention (for  $\sigma=1$ ) to the octant  $\{x \geq 0, y \geq 0, z \geq 0\}$ , keeping in mind that there is a symmetric IGW activity in the other three octants  $\{x \geq 0, y \geq 0, z \leq 0\}$ ,  $\{x \leq 0, y \leq 0, z \geq 0\}$  and  $\{x \leq 0, y \leq 0, z \leq 0\}$ .

Figures 2 and 3 summarize our results for  $\varepsilon=0.25$  and  $\sigma=1$ . They show  $\zeta_{\text{igw}}$  in horizontal  $(X, Y)$ -planes corresponding to the three altitudes  $Z=0$ ,  $Z=10$  and  $Z=20$  and for the times  $t=1, 2, \dots, 7$  (figure 2) and  $t=8, 9, 10$  (figure 3). The range of values of  $X$  is extended for the three later times to show the full extent of the IGWs radiated; for these times, the results on the plane  $Z=0$  are not shown since  $\zeta_{\text{igw}}$  has become weak at small altitudes. The smallest value of  $Y$  shown in the two figures is  $Y=1$  because we found it difficult to obtain smooth results for  $0 \leq Y < 1$  and  $Z=0$  when  $t \approx 3$ ; the switch between saddle and endpoint contributions to  $\zeta_{\text{igw}}$  is then quite abrupt.

To interpret the numerical values attained by  $\zeta_{\text{igw}}$ , it can be observed that the ratio  $\zeta_{\text{igw}}/\zeta_{\text{bal}}$  is unaffected by the scaling used for  $q_0$ , and that the numerical values obtained for  $\zeta_{\text{bal}}$  from (4.6) are of order one; the amplitude indicated by the grey scale in figures 2 and 3 can therefore be taken as an estimate for the inertia–gravity-wave activity relative to the balanced activity. It is worth emphasizing that because our approach is essentially analytic,  $\zeta_{\text{igw}}$  is obtained at each point in space and time in a

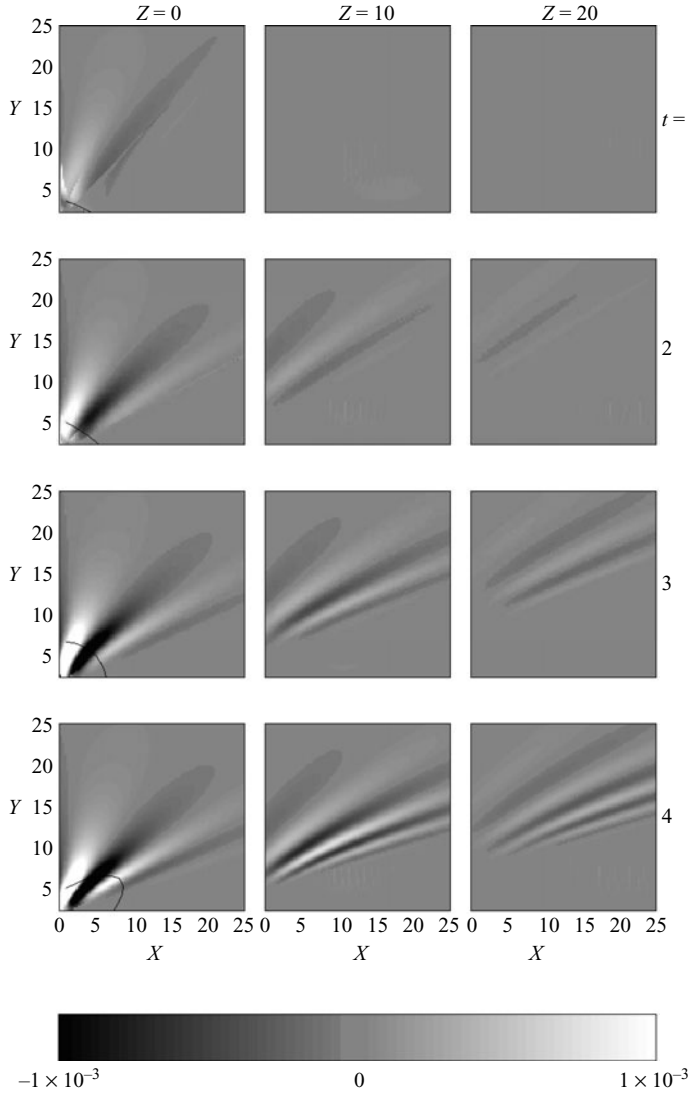


FIGURE 2. For caption see next page.

completely independent fashion, so the choice of time interval and spatial gridding is entirely dictated by visualization considerations.

The figures reveal how the sheared vortex (only a very small ellipsoid in the scaled coordinates employed) radiates four packets of comparatively large-scale IGWs (one in each of the four downstream octants). As expected, the bulk of the IGW radiation occurs around  $t = T = 3$ . At these early times, the IGW activity is confined near  $Z = 0$ , but the packets rapidly propagate vertically; as they do so, they are affected by the horizontal shear which tilts the phase lines towards the  $X$ -axis and reduces horizontal scales. The propagation and shearing of the IGWs is not the only part of the response to the vortex: in particular, at  $Z = 0$ , there is a clear stationary pattern for  $X < 10$ . Examination of our asymptotic evaluation of the integral (4.7) indicates that this stationary pattern arises from one of its endpoints, namely  $\tau = 0$ . This endpoint contribution corresponds to the sheared modes with  $l = \sigma k t$ , that is, to the modes

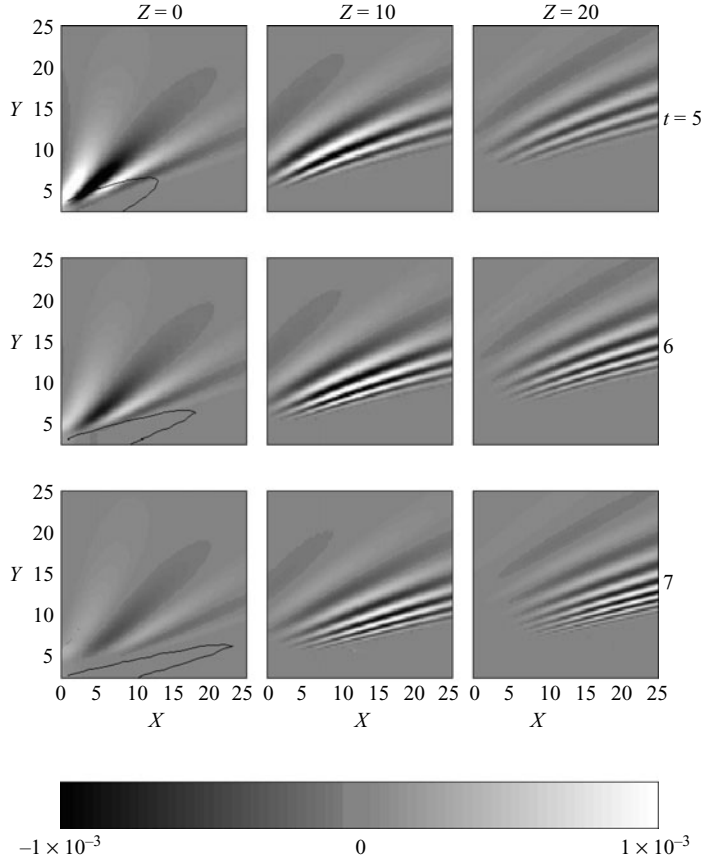


FIGURE 2. Vertical vorticity  $\zeta_{\text{igw}}$  associated with the IGWs radiated by an ellipsoidal vortex in an anticyclonic horizontal Couette flow. The parameters are  $\varepsilon = 0.25$  and  $T = 3$ , and the scaled spatial coordinates  $(X, Y, Z) = \varepsilon^{1/2}(x, y, Nz/f)$  are used.  $\zeta_{\text{igw}}$  is shown as a function of  $(X, Y)$ , for  $Z = 0, 10$  and  $20$  and for  $t = 1, 2, \dots, 7$ . The vortex is localized near the origin, with a typical size  $\varepsilon^{1/2} = 0.5$  in the scaled coordinates; its shape is indicated by the contour line corresponding to  $q = \exp(-30)$ .

whose IGW oscillations are precisely switched on at time  $t$ . The  $y$ -independent spatial structure of these modes (see e.g. (3.9)) explains why the stationary pattern makes only a small angle with the  $Y$ -axis. With its wider  $X$ -range, figure 3 demonstrates how dispersion spreads the packets as they propagate. Nevertheless, the evolution is largely dominated by advection, and most of the wavepacket energy surrounds the ray  $x + z = \sigma ty$ , as the asymptotic derivation of Appendix A suggests should be the case.

To conclude, we point out that we have carried out similar computations in the case of a cyclonic flow ( $\sigma = -1$ ). Apart from the obvious changes in the location of the wavepackets, always located downstream of the potential-vorticity ellipsoid, the structure of the IGWs is similar to that just described. A significant difference, however, is that the amplitude is smaller by an  $O(1)$  factor, as expected.

## 6. Discussion

In this paper, we have given an explicit description of the IGWs that are generated spontaneously by a simple balanced flow. The regime considered is the

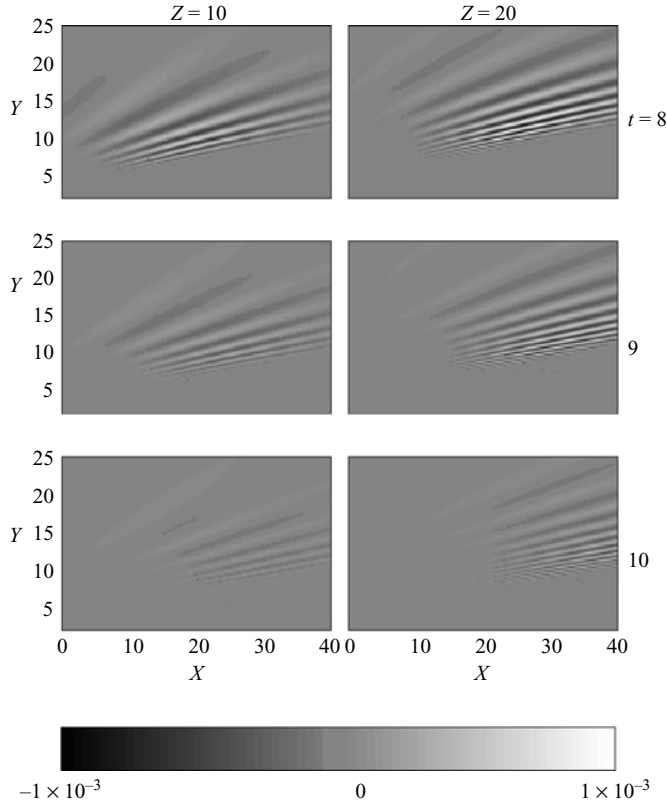


FIGURE 3. Same as figure 2, but for the later times  $t = 8, 9$  and  $10$ . The altitude  $Z = 0$ , where the IGW activity is weak, is not shown.

small-Rossby-number quasi-geostrophic regime where the IGWs can be expected to be exponentially small in the Rossby number. The exponential smallness has been demonstrated previously for models such as the Lorenz 5-component model (Lorenz & Krishnamurthy 1987; Vanneste 2004) and an extension thereof (Vanneste 2006). Our results show that it also holds in a more realistic context of localized solutions of the three-dimensional Boussinesq equations. The type of solution considered, consisting of a localized potential-vorticity perturbation superposed on a horizontal Couette flow, is very specific, and is guided by the possibility of a complete asymptotic treatment relying on an expansion in sheared modes. The results nonetheless usefully complement recent numerical work which gives examples of spontaneous generation of IGWs in more complicated and realistic flows but does not provide as clear-cut a description of the waves as that given here. The advantages of an asymptotic approach, when available, are evident when one considers the difficulties in initializing balanced flows and in extracting IGW fields from data that are typically encountered in numerical studies of IGW generation (see Viúdez & Dritschel 2004, for a technique addressing the difficulties). These are completely avoided here: the exponential-asymptotic approach allows us to define an initial state that is unambiguously free of IGWs, and to study the IGWs in isolation from the much stronger balanced motion. In view of these advantages, it would be highly desirable to develop exponential-asymptotic techniques that apply to a broader class of flows than that considered in this paper. This would require an approach that does not rely on the reduction

from partial to ordinary differential equations made possible here by the expansion in sheared modes.

One of the outcomes of our work is that the typical length scale of the IGWs radiated spontaneously depends on the Rossby number like  $\varepsilon^{-1/2}$ . That long waves are emitted is reminiscent of the situation in the small-Froude-number regime  $F \ll 1$ ,  $\varepsilon = O(1)$ , where the IGW wavelengths scale like  $F^{-1}$  (e.g. Ford *et al.* 2000; Plougonven & Zeitlin 2002). The physics behind the two scalings is rather different, however. In the small-Froude-number regime, the radiation can be attributed to a resonance between IGWs and balanced motion, and long waves are selected because their low frequencies match those of the balanced motion. In the small-Rossby-number regime  $\varepsilon \ll 1$ ,  $F = O(\varepsilon)$ , by contrast, frequency matching is impossible, whatever the wave scale. The wave amplitudes are then of the form  $\exp(-\alpha/\varepsilon)$ , where  $\alpha$  depends on the wavenumbers. The typical scales that emerge from the radiation process correspond to wavenumbers minimizing  $\alpha$ . Saddle-point arguments suggest that these should be in an  $O(\varepsilon^{1/2})$  neighbourhood of the origin, thus explaining (in a highly schematic manner) the  $O(\varepsilon^{-1/2})$  scales obtained. It should be noted that the IGWs observed in numerical simulations of spontaneous generation are typically short compared with the flow scale (e.g. O'Sullivan & Dunkerton 1995; Zhang 2004; Plougonven & Snyder 2005, 2007; Viúdez & Dritschel 2006; Viúdez 2006). One might speculate on the reasons for this and invoke, in particular, the presence in these simulations of active small-scale features in the balanced flow, or the possibility of unbalanced instabilities which typically involve small-scale waves (see Vanneste & Yavneh 2007, and references therein).

We conclude by returning to some of the assumptions that we made, and discuss how they may be relaxed. A first assumption is the adoption of the hydrostatic approximation. This is made for convenience only, since the explicit form (4.2) for the IGW-component of sheared modes can be generalized to the non-hydrostatic case using the results of Vanneste & Yavneh (2004). We note that relaxing the hydrostatic approximation is necessary if the large-time behaviour of the IGWs is to be modelled accurately: because of the increase in the cross-stream wavenumber  $|l| \approx |\Sigma kt|$ , the horizontal wavenumber is only negligible compared to the vertical one in the IGW dispersion relation if  $t \ll N/(\Sigma f)$  (recall that the dominant wavenumbers satisfy  $\beta = fm/(Nk) \approx 1$ ). However, the asymptotic evaluation of the integral giving  $\zeta_{\text{igw}}$  would be considerably more difficult without the hydrostatic approximation, notably because the generalization of (4.2) has a complicated form, involving elliptic integrals rather than elementary functions.

A second assumption is that of an ellipsoidal potential-vorticity distribution. This was made for definiteness, and any localized potential vorticity could in principle be chosen, although analytical progress with the resulting integral form of  $\zeta_{\text{igw}}$  will only be possible for simple enough choices. An interesting choice, in view of the sharp potential-vorticity gradients often observed in the atmosphere and oceans, would be that of a piecewise-constant potential vorticity, and in particular of a patch of uniform potential vorticity. For an ellipsoidal patch, preliminary computations suggest that two integrations could be carried out analytically, as is the case in this paper. The asymptotic evaluation of the second differs entirely from the one presented here and would require careful consideration. Nonetheless, we can already remark that a piecewise-constant potential vorticity does not affect the conclusion that the IGWs generated spontaneously are exponentially small in the Rossby number. Thus spatial smoothness does not appear essential for exponential smallness, unlike temporal smoothness which is, of course, critical.

Finally, our results rely on the linearization of the dynamics of perturbations to the horizontal Couette flow. This approximation is critical in two respects: first, it reduces the evolution of the potential vorticity to a simple advection by a known flow, and second it makes it possible to treat the perturbation as a superposition of sheared modes and hence to reduce the dynamics to ordinary differential equations. Treating a fully nonlinear problem would require not only obtaining an approximation to the potential-vorticity dynamics that is valid to all orders in the Rossby number, but also developing exponential-asymptotic techniques for partial-differential equations.

J. V. was funded by a NERC Advanced Research Fellowship.

## Appendix A. Evaluation of $\zeta_{\text{igw}}$

This Appendix details the method employed to estimate the triple integral (4.7) giving the IGW part of the vertical vorticity  $\zeta_{\text{igw}}$  for the initial potential vorticity (2.8).

### A.1. Formulation

A first step is to change the integration variables from  $(k, l, m)$  to  $(k, \tau, \beta)$  with  $\tau = t - \sigma l/k$ . Noting that the Jacobian of the transformation is  $Nk^2/f$  and we find after some calculations that

$$\zeta_{\text{igw}}(x, y, z, t) = 2 \int_{-\infty}^{\infty} \int_0^t \tilde{\zeta}_{\text{igw}}(\beta, \tau) \int_0^{\infty} k^2 e^{-A(\beta, \tau)k^2} \cos[B(\beta, \tau)k] dk d\tau d\beta, \quad (\text{A } 1)$$

where

$$A(\beta, \tau) = \alpha_1^2 + \alpha_2^2(\tau - t + T)^2 + \alpha_3^2 N^2 \beta^2 / f^2 \quad \text{and} \quad B(\beta, \tau) = x - \sigma \tau y + \beta N z / f. \quad (\text{A } 2)$$

We remark that these expressions indicate that a natural vertical coordinate is  $Nz/f$ , as is usual with the quasi-geostrophic scaling used in this paper. Since  $\tilde{\zeta}_{\text{igw}}$  is independent of  $k$ , we can carry out the integration with respect to  $k$  explicitly to find that

$$\begin{aligned} \zeta_{\text{igw}}(x, y, z, t) &= \sqrt{\pi} \int_{-\infty}^{\infty} \int_0^t \tilde{\zeta}_{\text{igw}}(\beta, \tau) e^{-B^2(\beta, \tau)/(4A(\beta, \tau))} \\ &\quad \times \left( \frac{1}{2A^{3/2}(\beta, \tau)} - \frac{B^2(\beta, \tau)}{4A^{5/2}(\beta, \tau)} \right) d\tau d\beta. \end{aligned}$$

Because  $\tilde{\zeta}_{\text{igw}}$  depends on  $\tau$  and  $\beta$  in a complicated manner (see (4.2)), it is not possible to perform further explicit integrations. We can however take advantage of the smallness of  $\varepsilon$  to approximate  $\zeta_{\text{igw}}$ .

To estimate the small- $\varepsilon$  behaviour of the inner integral

$$I_\beta(x, y, z, t) = \sqrt{\pi} \int_0^t \tilde{\zeta}_{\text{igw}}(\beta, \tau) e^{-B^2(\beta, \tau)/(4A(\beta, \tau))} \left( \frac{1}{2A^{3/2}(\beta, \tau)} - \frac{B^2(\beta, \tau)}{4A^{5/2}(\beta, \tau)} \right) d\tau,$$

we substitute the function  $\tilde{\zeta}_{\text{igw}}$  by its leading behaviour (4.2). Writing the sine and cosine as sums of imaginary exponentials, this gives the asymptotic relation

$$I_\beta(x, y, z, t) \sim \text{Im} \int_0^t g(\beta, \tau, \varepsilon) e^{-f(\beta, \tau)/\varepsilon} d\tau, \quad (\text{A } 3)$$



where

$$f(\beta, \tau) = \varepsilon \frac{B^2(\beta, \tau)}{4A(\beta, \tau)} + \frac{\pi}{4} \left( \frac{1}{|\beta|} + |\beta| \right) + \frac{i}{2|\beta|} \left( \tau \sqrt{1 + \beta^2 + \tau^2} + (1 + \beta^2) \ln \left( \frac{\tau + \sqrt{1 + \beta^2 + \tau^2}}{\sqrt{1 + \beta^2}} \right) \right), \quad (\text{A } 4)$$

$$g(\beta, \tau, \varepsilon) = -\pi \sqrt{\frac{2|\beta|}{\varepsilon}} \frac{\sqrt{1 + \tau^2}}{(1 + \beta^2 + \tau^2)^{1/4} (1 + \beta^2)^{1/4}} \left( \frac{1}{2A(\beta, \tau)} - \frac{B^2(\beta, \tau)}{4A^{5/2}(\beta, \tau)} \right) e^{-h(\beta, \tau)}, \quad (\text{A } 5)$$

and

$$h(\beta, \tau) = -\sigma \left( \frac{\pi|\beta|}{4} + \frac{i|\beta|}{2} \ln \left( \frac{\tau + \sqrt{1 + \beta^2 + \tau^2}}{\sqrt{1 + \beta^2}} \right) + i \arcsin \left( \frac{|\beta|\tau}{\sqrt{1 + \beta^2} \sqrt{1 + \tau^2}} \right) \right). \quad (\text{A } 6)$$

We have written the integral (A 3) in the form of a Laplace integral. In doing so, we have treated the first term in  $f(\beta, \tau)$  as an  $O(1)$  term in spite of the explicit factor  $\varepsilon$ . This is because a distinguished limit is achieved in (A 3), and the largest values of  $I_\beta$  are attained, when  $(x, y, z)$  are of order  $\varepsilon^{-1/2}$  and hence  $B^2 = O(\varepsilon^{-1})$  in the first term of  $f(\beta, \tau)$ . In what follows, we will therefore treat  $\varepsilon^{1/2}(x, y, z)$  as  $O(1)$  parameters, but we will also retain terms necessary for our estimate of (A 3) to be valid uniformly when  $B = O(1)$ .

The integral (A 3) can be dominated by the saddle point of  $f(\beta, \tau)$ , by one of the endpoints of the interval of integration, or simultaneously by the saddle and one of the endpoints. To handle this behaviour in a continuous manner, a uniform asymptotic method is called for; we use Bleistein's (1966) method which is designed to uniformly combine the contributions from an endpoint and from a saddle point in an integral. Details of this method are presented in Appendix B. There we show that if the dominant endpoint is  $\tau_e = 0$  and the saddle point of  $f(\beta, \tau)$  is  $\tau_s$ , a uniform approximation to (A 3) is

$$I_\beta(x, y, z, t) \sim \text{Im} \left\{ e^{-b/\varepsilon} \left[ \sqrt{\frac{\pi\varepsilon}{2}} e^{a^2/(2\varepsilon)} \left( 1 + \text{erf} \left( \frac{a}{\sqrt{2\varepsilon}} \right) \right) (\alpha_0 + \alpha_1 \varepsilon) + (\beta_0 + \beta_1 \varepsilon) \varepsilon \right] \right\}, \quad (\text{A } 7)$$

where  $a$  and  $b$  satisfy

$$f(\tau_e) = b, \quad f(\tau_s) = b - \frac{a^2}{2},$$

and  $\alpha_0, \beta_0, \alpha_1$  and  $\beta_1$  are defined in terms  $f$  and  $g$  in (B 7)–(B 8) and (B 11)–(B 12).

Note that we have included the first two terms in the expansion near each of the saddle point and endpoint: this proves necessary to obtain an approximation accurate over a wide enough range of values of  $(x, y, z, t)$ . When the saddle point  $\tau_s$  is close to the other endpoint  $\tau_e = t$  we obtain an analogous approximation as explained in Appendix B.

Note also that there is no explicit analytic expression for the (complex) saddle point  $\tau_s$ , but that it can always be found numerically. It is therefore possible to compute the value of  $I_\beta$  from (A 7) numerically, as is required for the subsequent numerical integration over  $\beta$ .

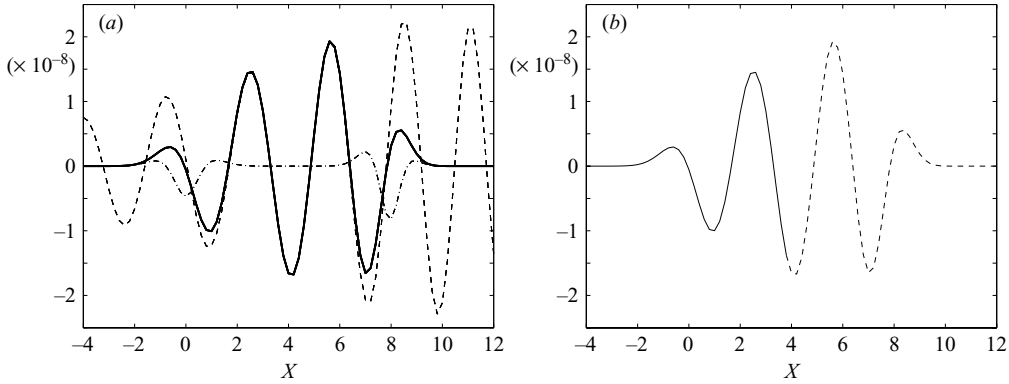


FIGURE 4. Integral  $I_\beta$  as a function of  $X = \varepsilon^{1/2}x$  for  $\varepsilon = 0.1$ ,  $\sigma = -1$ ,  $Y = \varepsilon^{1/2}y = 8$ ,  $z = 0$ ,  $t = 1$  and  $T = 0$ . (a) Comparison of a numerical evaluation of  $I_\beta$  (solid line) with asymptotic estimates giving the endpoint contribution (dash-dotted line) and saddle-point contribution (dashed line). (b) The estimate obtained using Bleistein's method uniformly combining the contributions from the saddle point and from the endpoint  $\tau_e = 0$  (solid line) or  $\tau_e = t$  (dashed line).

Figure 4 demonstrates the validity of the estimate (A 7) and the usefulness of Bleistein's method. It compares a numerical evaluation of  $I_\beta$  with several asymptotic estimates as a function of  $X = \varepsilon^{1/2}x$  for  $\varepsilon = 0.1$  and other parameters fixed. Figure 4(a) illustrates the shortcomings of using separately the saddle-point and endpoint contributions. Figure 4(b) validates the use of Bleistein's method applied with either the endpoint  $\tau_e = 0$  or  $\tau_e = t$ .

#### A.2. Numerical implementation

We proceed as follows for the numerical computation of  $\zeta_{\text{igw}}$ . For fixed  $x$ ,  $y$ ,  $z$  and  $t$ , we find the saddle point  $\tau_s$  numerically for each value of  $\beta$  and then compute an approximation to  $I_\beta$  using Bleistein's method. We use either  $\tau_e = 0$  or  $\tau_e = t$  as the endpoint for Bleistein's method, depending on which is closer to the saddle. Integrating the approximated values of  $I_\beta$  numerically using Simpson's method gives an approximation of  $\zeta_{\text{igw}}$ . The integration range for  $\beta$  is infinite, but we can integrate over a finite range using the fact that  $I_\beta$  is strongly peaked in the neighbourhood of  $|\beta| = 1$ , as can be expected from the second term in (A4).

The computations can be minimized by taking advantage of some symmetries: it is easy to check that

$$I_\beta(x, -y, z, \beta, t) = I_\beta(-x, y, -z, \beta, t), \quad (\text{A } 8)$$

$$I_\beta(x, y, -z, \beta, t) = I_\beta(x, y, z, -\beta, t), \quad (\text{A } 9)$$

and hence that

$$\zeta_{\text{igw}}(x, -y, z, t) = \zeta_{\text{igw}}(-x, y, -z, t), \quad (\text{A } 10)$$

$$\zeta_{\text{igw}}(x, y, -z, t) = \zeta_{\text{igw}}(x, y, z, t). \quad (\text{A } 11)$$

Thus we can restrict our efforts to the region  $x \geq 0$  and  $z \geq 0$ . Computations can be further reduced by exploiting the fact that the integrand of  $I_\beta$  depends on  $x$  and  $z$  through  $x + \beta z$  only. Finally, we note that non-negligible values of  $I_\beta$  are essentially restricted to the regions between the rays  $x + \beta z = 0$  and  $x + \beta z = \sigma ty$ . Since  $I_\beta$  is dominated by values of  $|\beta|$  near 1, this means that the IGW response is mainly confined between the rays  $x + z = 0$  and  $x + z = \sigma ty$ . Certainly, there is hardly

any response upstream of the flow, hence we restrict computations to the octant  $\{x \geq 0, \sigma y \geq 0, z \geq 0\}$ .

## Appendix B. Bleistein's method

Bleistein's method (Bleistein 1966) provides an asymptotic expansion for Laplace-type integrals of the form

$$I(t) = \int_0^t g(\tau, \varepsilon) e^{-f(\tau)/\varepsilon} d\tau, \quad (\text{B } 1)$$

whose main contribution comes from a saddle point of  $f(\tau)$  and from an endpoint of the integration range. This method uniformly combines the contributions from the saddle point and endpoint, and it is particularly useful when the two points coalesce as a parameter changes.

The idea of Bleistein's method is to write an approximation to  $I(t)$  of the form

$$\int_0^\infty e^{-(w^2/2 - aw + b)/\varepsilon} h(w) dw,$$

where a new variable  $w$  is introduced such that  $w = a$  corresponds to the saddle point  $\tau_s$  of  $f$ , and  $w = 0$  corresponds to the relevant endpoint,  $\tau_e$ , which we take as  $\tau_e = 0$  in the derivation. Comparing with (B 1) gives

$$f(\tau) = \frac{w^2}{2} - aw + b, \quad (\text{B } 2)$$

and

$$f(\tau_e) = b \quad \text{and} \quad f(\tau_s) = b - \frac{a^2}{2}. \quad (\text{B } 3)$$

It follows that

$$a = \pm \sqrt{2(f(\tau_e) - f(\tau_s))}, \quad (\text{B } 4)$$

which can be considered as a measurement of the distance between the values of  $f$  at the saddle and the endpoint. The sign of  $a$  is chosen in order to ensure that the order of the endpoints and saddle is identical in the coordinates  $\tau$  and  $w$ .

With this notation,

$$\begin{aligned} \int_0^t g(\tau, \varepsilon) e^{-f(\tau)/\varepsilon} d\tau &= \int_0^{w(t)} e^{-(w^2/2 - aw + b)/\varepsilon} g(\tau(w)) \frac{d\tau}{dw} dw \\ &= \int_0^{w(t)} e^{-(w^2/2 - aw + b)/\varepsilon} h_0(w) dw, \end{aligned} \quad (\text{B } 5)$$

where  $w(t)$  corresponds to the endpoint  $t$  and  $h_0(w) = g(\tau(w)) d\tau/dw$ . Next, we expand  $h_0(w)$  around the saddle point and the endpoint simultaneously by writing

$$h_0(w) = \alpha_0 + \beta_0(w - a) + w(w - a)k_0(w), \quad (\text{B } 6)$$

where the coefficient  $\alpha_0$  represents the expansion around  $w = a$  and the coefficient  $\beta_0$  represents the expansion around  $w = 0$ . Hence we take

$$\alpha_0 = h_0(a) \quad \text{and} \quad \beta_0 = \frac{h_0(a) - h_0(0)}{a}.$$

Now, differentiating equation (B 2) with respect to  $w$  and noting that  $w = a$  corresponds to  $\tau = \tau_s$  leads to

$$\left. \frac{d\tau}{dw} \right|_{w=a} = \lim_{w \rightarrow a} \frac{(w-a)}{df/d\tau} = \lim_{w \rightarrow a} \frac{(w-a)}{f''(\tau_s)(\tau - \tau_s)} = \frac{1}{f''(\tau_s) d\tau/dw|_{w=a}},$$

so that

$$\alpha_0 = h_0(a) = \frac{g(\tau_s)}{\sqrt{f''(\tau_s)}}. \quad (\text{B } 7)$$

Similarly,

$$\beta_0 = \frac{h_0(a) - h_0(0)}{a} = \frac{g(\tau_s)}{a\sqrt{f''(\tau_s)}} + \frac{g(0)}{f'(0)}. \quad (\text{B } 8)$$

We are now in position to estimate  $I(t)$ . Introducing (B 6) in (B 5) and extending the integration range to infinity we obtain, after integration by parts,

$$\begin{aligned} I(t) \sim e^{-b/(2\varepsilon)} & \left[ \alpha_0 \sqrt{\frac{\pi\varepsilon}{2}} e^{a^2/(2\varepsilon)} \left( 1 + \operatorname{erf} \left( \frac{a}{\sqrt{2\varepsilon}} \right) \right) + \beta_0 \varepsilon \right] \\ & + \varepsilon \int_0^\infty e^{-(w^2/2 - aw + b)/\varepsilon} \frac{d}{dw} (wk_0(w)) dw. \end{aligned} \quad (\text{B } 9)$$

The remaining integral is  $O(\varepsilon^{3/2})$  and hence in principle negligible. However, for the problem in this paper, we found that the accuracy of the first two terms was not sufficient to provide reliable results with typical relevant values of  $\varepsilon$  and the range of parameters considered. We therefore derive additional terms in the asymptotic expansion of the integral  $I(t)$ .

To find a third term in the expansion, we expand the integrand of the integral remaining in (B 9) around  $w=0$  and  $w=a$  in the same manner as before. Thus, we write

$$h_1(w) = \frac{d}{dw} (wk_0(w)) = \alpha_1 + \beta_1(w-a) + w(w-a)k_1(w), \quad (\text{B } 10)$$

where

$$\alpha_1 = h_1(a) \quad \text{and} \quad \beta_1 = \frac{h_1(a) - h_1(0)}{a}.$$

In terms of the function  $h_0(w)$  these coefficients are

$$\left. \begin{aligned} \alpha_1 &= \frac{1}{2} h_0''(a), \\ \beta_1 &= \frac{\frac{1}{2} a^2 h_0''(a) - h_0(a) + h_0(0) + a h_0'(0)}{a^3} = \frac{a\alpha_1 - \beta_0 + h_0'(0)}{a^2}. \end{aligned} \right\} \quad (\text{B } 11)$$

To compute them, we use similar methods as before to obtain

$$\left. \begin{aligned} h_0'(0) &= a^2 \frac{g'(0)f'(0) - g(0)f''(0)}{f'(0)^3} + \frac{g(0)}{f'(0)} \\ h_0''(a) &= \frac{12g''(\tau_s)f''(\tau_s)^2 - 12g'(\tau_s)f''(\tau_s)f'''(\tau_s) - 3g(\tau_s)f''(\tau_s)f^{(4)}(\tau_s) + 5g(\tau_s)f'''(\tau_s)^2}{12[f''(\tau_s)]^{7/2}}. \end{aligned} \right\} \quad (\text{B } 12)$$

Substituting  $h_1(w)$  in (B 9) by its expansion (B 10) then gives

$$I(t) \sim e^{-b/(2\varepsilon)} \left[ \sqrt{\frac{\pi\varepsilon}{2}} e^{a^2/(2\varepsilon)} \left( 1 + \operatorname{erf} \left( \frac{a}{\sqrt{2\varepsilon}} \right) \right) (\alpha_0 + \alpha_1\varepsilon) + (\beta_0 + \beta_1\varepsilon)\varepsilon \right] \\ + \varepsilon^2 \int_0^\infty e^{-(w^2/2 - aw + b)/\varepsilon} \frac{d}{dw} (wk_1(w)) dw,$$

where the remaining integral now contributes at  $O(\varepsilon^{5/2})$ .

Further terms in the asymptotic expansion could be obtained by expanding successively the derivative of the functions  $k_n$ . This is Bleistein's method, giving a recursive scheme to find an asymptotic expansion of the integral. In this paper we neglect the  $O(\varepsilon^{5/2})$  terms and hence ignore the integral remaining in (B 13).

When the saddle point  $\tau_s$  is close to the other endpoint  $\tau_e = t$  we derive an analogous approximation by substituting  $(t - \tau)$  for  $\tau$  in the expressions above. This amounts to changing  $b$  from  $b = f(\tau_e = 0)$  to  $b = f(\tau_e = t)$ , adjusting the value of  $a$  accordingly and, substituting  $f^{(n)}(\tau_s)$  by  $(-1)^n f^{(n)}(\tau_s)$  and  $g^{(n)}(\tau_s)$  by  $(-1)^n g^{(n)}(\tau_s)$  in the coefficients  $\alpha_i$  and  $\beta_i$ .

#### REFERENCES

- BABIN, A., MAHALOV, A. & NICOLAENKO, B. 2000 Fast singular oscillating limits and global regularity for the 3D primitive equations of geophysics. *Math. Model. Numer. Anal.* **34**, 201–222.
- BERRY, M. V. 1989 Uniform asymptotic smoothing of Stokes's discontinuities. *Proc. R. Soc. Lond. A* **422**, 7–21.
- BLEISTEIN, N. 1966 Uniform asymptotic expansions of integrals with stationary point near algebraic singularity. *Commun. Pure Appl. Maths* **19**, 353–370.
- FORD, R., MCINTYRE, M. E. & NORTON, W. A. 2000 Balance and the slow quasi-manifold: some explicit results. *J. Atmos. Sci.* **57**, 1236–1254.
- FRITTS, D. C. & ALEXANDER, M. J. 2003 Gravity wave dynamics and effects in the middle atmosphere. *Rev. Geophys.* **41**, 000106.
- LORENZ, E. N. & KRISHNAMURTHY, V. 1987 On the nonexistence of a slow manifold. *J. Atmos. Sci.* **44**, 2940–2950.
- MAJDA, A. J. & EMBID, P. 1998 Averaging over fast gravity waves for geophysical flows with unbalanced initial data. *Theor. Comput. Fluid Dyn.* **11**, 155–169.
- MCWILLIAMS, J. C. & YAVNEH, I. 1998 Fluctuation growth and instability associated with a singularity of the balance equations. *Phys. Fluids* **10**, 2587–2596.
- ÓLAFSDÓTTIR, E. I., OLDE DAALHUIS, A. B. & VANNESTE, J. 2005 Stokes-multiplier expansion in an inhomogeneous differential equation with a small parameter. *Proc. R. Soc. Lond. A* **461**, 2243–2256.
- O'SULLIVAN, D. & DUNKERTON, T. J. 1995 Generation of inertia-gravity waves in a simulated life-cycle of baroclinic instability. *J. Atmos. Sci.* **52**, 3695–3716.
- PLOUGONVEN, R. & SNYDER, C. 2005 Gravity waves excited by jets: propagation versus generation. *Geophys. Res. Lett.* **32**, L18802.
- PLOUGONVEN, R. & SNYDER, C. 2007 Inertia-gravity waves spontaneously excited by jets and fronts. Part I: different baroclinic life cycles. *J. Atmos. Sci.* **64**, 2502–2520.
- PLOUGONVEN, R. & ZEITLIN, V. 2002 Internal gravity wave emission from a pancake vortex: an example of wave-vortex interaction in strongly stratified flows. *Phys. Fluids* **14**, 1259–1268.
- REZNIK, G. M., ZEITLIN, V. & BEN JELLOUL, M. 2001 Nonlinear theory of geostrophic adjustment. Part 1. Rotating shallow-water model. *J. Fluid Mech.* **445**, 93–120.
- VANNESTE, J. 2004 Inertia-gravity-wave generation by balanced motion: revisiting the Lorenz-Krishnamurthy model. *J. Atmos. Sci.* **61**, 224–234.
- VANNESTE, J. 2006 Wave radiation by balanced motion in a simple model. *SIAM J. Appl. Dyn. Syst.* **5**, 783–807.

- VANNESTE, J. 2008 Exponential smallness of inertia–gravity-wave generation at small Rossby number. *J. Atmos. Sci.* In press.
- VANNESTE, J. & YAVNEH, I. 2004 Exponentially small inertia–gravity waves and the breakdown of quasi-geostrophic balance. *J. Atmos. Sci.* **61**, 211–223.
- VANNESTE, J. & YAVNEH, I. 2007 Unbalanced instabilities of rapidly rotating stratified shear flows. *J. Fluid Mech.* **584**, 373–396.
- VIÚDEZ, A. 2006 Spiral patterns of inertia–gravity waves in geophysical flows. *J. Fluid Mech.* **562**, 73–82.
- VIÚDEZ, A. & DRITSCHER, D. G. 2004 Optimal potential vorticity balance of geophysical flows. *J. Fluid Mech.* **521**, 343–352.
- VIÚDEZ, A. & DRITSCHER, D. G. 2006 Spontaneous emission of inertia–gravity wave packets by balanced geophysical flows. *J. Fluid Mech.* **553**, 107–117.
- WARN, T. 1997 Nonlinear balance and quasi-geostrophic sets. *Atmos. Oceans* **35**, 135–145.
- WARN, T., BOKHOVE, O., SHEPHERD, T. G. & VALLIS, G. K. 1995 Rossby number expansions, slaving principles, and balance dynamics. *Q. J. R. Met. Soc.* **121**, 723–739.
- ZHANG, F. 2004 Generation of mesoscale gravity waves in upper-tropospheric jet-front systems. *J. Atmos. Sci.* **61**, 440–457.